

000 001 002 003 004 005 006 007 008 009 010 011 012 013 014 015 016 017 018 019 020 021 022 023 024 025 026 027 028 029 030 031 032 033 034 035 036 037 038 039 040 041 042 043 044 045 046 047 048 049 050 051 052 053 GEO-R1: IMPROVING FEW-SHOT GEOSPATIAL RE- FERRING EXPRESSION UNDERSTANDING WITH REIN- FORCEMENT FINE-TUNING

006 **Anonymous authors**

007 Paper under double-blind review

011 ABSTRACT

013 Referring expression understanding in remote sensing poses unique challenges,
014 as it requires reasoning over complex object–context relationships. While su-
015 pervised fine-tuning (SFT) on multimodal large language models achieves strong
016 performance with massive labeled datasets, they struggle in data-scarce scenarios,
017 leading to poor generalization. To address this limitation, we propose Geo-R1, a
018 reasoning-centric reinforcement fine-tuning (RFT) paradigm for few-shot geospa-
019 tial referring. Geo-R1 enforces the model to first generate explicit, interpretable
020 reasoning chains that decompose referring expressions, and then leverage these
021 rationales to localize target objects. This “reason first, then act” process enables
022 the model to make more effective use of limited annotations, enhances gener-
023 alization, and provides interpretability. We validate Geo-R1 on three carefully
024 designed few-shot geospatial referring benchmarks, where our model consistently
025 and substantially outperforms SFT baselines. It also demonstrates strong cross-
026 dataset generalization, highlighting its robustness. Code and data will be released
027 at <http://geo-r1.github.io>.

028 1 INTRODUCTION

030 Vision language models (VLMs) have become a critical tool for remote sensing imagery (RSI) un-
031 derstanding (Li et al., 2024d; Weng et al., 2025). By coupling natural language with RSI, VLMs
032 can drive a wide spectrum of tasks in the RS domain, such as image captioning, visual question an-
033 swering, referring expression comprehension (REC), referring expression segmentation (RES) (Li
034 et al., 2024d; Zhou et al., 2024a). Among these capabilities, REC and RES tasks are especially im-
035 portant: both require the model to resolve free-form linguistic descriptions (e.g., “a small vehicle is
036 situated at the bottom right adjacent to a large vehicle”) into concrete, spatially localized predictions
037 (bounding boxes or segmentation masks) in high-resolution aerial images. We henceforth use the
038 term *Referring Expression Understanding* (REU) to denote a unified framework encompassing both
039 REC and RES, where the task is to take an image and a text query as input and output one or more
040 target objects.

041 Although recent works (Kuckreja et al., 2024; Yuan et al., 2024; Zhou et al., 2024b) have achieved
042 remarkable progress on REU tasks with supervised finetuning (SFT), these methods are highly de-
043 pendent on large-scale training labels. High-quality REU supervision demands not only image-level
044 labels but also precise language–region alignment at the object and region levels. Creating such
045 associations in overhead imagery requires expertise and careful tooling: annotators must parse com-
046 plex scene layouts, disambiguate visually similar man-made structures, and write unambiguous re-
047 ferring expressions before drawing spatially accurate boxes or masks. Compared with image-level
048 labels, these fine-grained annotations are orders of magnitude more labor-intensive. For example,
049 VRSBench (Li et al., 2024c) costs 1,004 labor hours for label verification only.

050 This reality makes few-shot learning (e.g., only 10 samples are provided for each category) in REU
051 valuable. Previous works, such as RS-CLIP(Li et al., 2023) and RemoteCLIP (Liu et al., 2024a)
052 have demonstrated that finetuning CLIP (Radford et al., 2021) on a few samples can yield strong
053 results for scene classification. However, these advances cannot be directly carried over to REU
since region-level grounding is harder than scene-level classification. Moreover, object relations

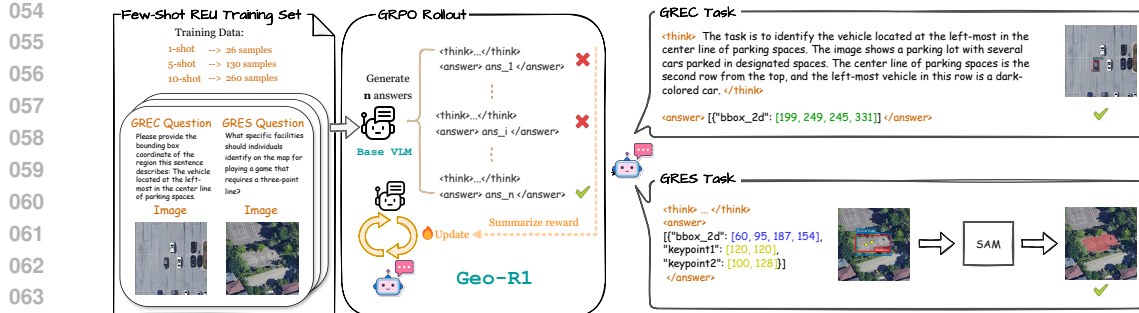


Figure 1: Geo-R1 method overview. Geo-R1 is trained on a few labeled samples with reinforcement learning (e.g., GRPO (Shao et al., 2024)) and can identify target objects (bounding boxes or masks) from an input image and text query while providing the reasoning process.

are complex for REU, requiring relational reasoning and disambiguation among visually similar structures. This raises the question: *with only a handful of aligned examples for each category, can a VLM learn to accurately ground language in remote sensing images?*

Driven by the impressive reasoning capabilities of OpenAI o1 (Jaech et al., 2024) and DeepSeek-R1 (Guo et al., 2025), reinforcement learning (RL) has become a powerful post-training paradigm for augmenting the reasoning capabilities of LLMs during post-training. RL explicitly encourages intermediate “thinking” steps, and forces the model learns to reason before committing to a prediction. This reasoning-first behavior is particularly well suited to few-shot REU: reasoning steps (e.g., “My intuition leads me to identify the vehicle sitting in the circular opening near the roadway as the small vehicle.”) serve as a transferable experience that generalizes better across different text-image samples than directly outputting a box/mask from next-token-prediction supervision.

In this work, we introduce a reasoning-centric RL post-training method, Geo-R1, which leverages task-specific reward functions to address few-shot REU. Geo-R1 encourages the model to generate explicit reasoning—intermediate hypotheses that parse the referring expression, identify contextual anchors, and iteratively refine localization—thereby regularizing learning and improving generalization. Unlike SFT, which relies on a single teacher-forced trajectory with a differentiable surrogate loss, Geo-R1 explores multiple reasoning chains and proposals, extracting advantages from N -way comparisons to provide denser and richer supervision per example, making better use of few-shot samples. Moreover, for RES, Geo-R1 directly optimizes a task-aligned *MaskGIoU* reward through the non-differentiable “BBox + SAM” pipeline (Ravi et al., 2025), enabling end-to-end training for dense prediction—a capability infeasible under SFT. Method overview can be found in Fig. 1.

In our experiments, we observe three consistent advantages from RL over SFT baselines for few-shot REU in remote sensing images. (1) With the same small number of labeled examples, our RFT-based reasoning model substantially outperforms SFT-based models on few-shot REU tasks. (2) In cross-dataset evaluation, our RFT-based model remarkably outperforms SFT counterparts, suggesting the reasoning model has stronger cross-dataset generalization than non-reasoning models. (3) The learned reasoning traces are useful and reasonable, utilizing the spatial and semantic cues that benefit the final localization, which provides a great interpretability. We further establish three few-shot benchmarks and define a few-shot protocol for REU. In summary, our contributions are listed below:

- To the best of our knowledge, we are the first to explore Referring Expression Understanding (REU) for aerial image understanding under few-shot settings. To facilitate rigorous and reproducible evaluation, we create VRSBench-FS, EarthReason-FS, and NWPU-FS, establishing standardized protocols for few-shot REU in remote sensing.
- We define task-aligned rewards and a reasoning-centric RL recipe, including BBoxIoU reward for REC and a MaskGIoU reward for RES. We introduce the RL-trained reasoning models (Geo-R1) that generate concise grounding rationales for these tasks.

108 • Across all three benchmarks, our Geo-R1 models consistently outperform SFT under identical
 109 few-shot budgets, while exhibiting stronger generalization across datasets and providing human-
 110 auditable reasoning traces that explain successes and failures.

112 **2 TASK AND METHODOLOGY**

114 This section details the adaptation of the GRPO algorithm from language-only tasks to vision-
 115 language tasks. Then, we introduce and formally define the REU task under few-shot settings.
 116 Finally, we discuss how to apply GRPO to these tasks with customized task-specific reward func-
 117 tions.

119 **2.1 GRPO: FROM LLM TO VLM**

121 Group Relative Policy Optimization (GRPO) (Shao et al., 2024) is a reinforcement learning frame-
 122 work that removes the dependence on a value model and instead utilizes rule-based reward functions.
 123 The GRPO algorithm begins by sampling N candidate outputs $\{o_1, \dots, o_N\}$ from the current pol-
 124 icy model π_θ for a given query prompt q . Each response o_i is then evaluated by a reward function
 125 $R(q, o_i)$ to obtain a raw reward score r_i . To measure the relative quality of each response within
 126 the sampled group, GRPO standardizes the raw rewards to obtain the advantage value, as shown in
 127 Eq. 1. The advantage value \hat{A}_i denotes the normalized advantage of the response o_i relative to other
 128 samples within the group.

$$\hat{A}_i = \frac{r_i - \text{mean}\{r_1, r_2, \dots, r_N\}}{\text{std}\{r_1, r_2, \dots, r_N\}} \quad (1)$$

131 The policy π_θ is updated with a training objective (Eq. 2), designed to encourage the generation of
 132 responses with higher advantages.

$$\mathcal{J}_{\text{GRPO}}(\theta) = \mathbb{E}_{\{o_i\}_{i=1}^N \sim \pi_{\theta_{\text{old}}}(\cdot|q)} \left[\frac{1}{N} \sum_{i=1}^N \left(\min \left(c_1 \cdot \hat{A}_i, c_2 \cdot \hat{A}_i \right) - \beta D_{\text{KL}}(\pi_\theta || \pi_{\text{ref}}) \right) \right], \quad (2)$$

136 where

$$c_1 = \frac{\pi_\theta(o_i | q)}{\pi_{\theta_{\text{old}}}(o_i | q)}, c_2 = \text{clip}\left(\frac{\pi_\theta(o_i | q)}{\pi_{\theta_{\text{old}}}(o_i | q)}, 1 - \varepsilon, 1 + \varepsilon\right). \quad (3)$$

139 Here, $D_{\text{KL}}(\pi_\theta || \pi_{\text{ref}})$ denotes the KL divergence between the current policy π_θ and the reference pol-
 140 icy π_{ref} , which serves as a regularization term to prevent large deviations. The clipping mechanism
 141 in c_2 stabilizes training by constraining the policy update ratio.

142 For LLMs on tasks with definitive answers, like mathematical reasoning, the reward can be cal-
 143 culated using a rule-based verifiable reward function. Building on GRPO, DeepSeek-R1 (Guo et al.,
 144 2025) demonstrates that such rewards enable models to produce both final answers and coherent rea-
 145 soning traces. This approach has been successfully extended to VLMs by converting visual metrics
 146 into tailored reward signals (Shen et al., 2025; Liu et al., 2025a;b).

148 **2.2 FEW-SHOT REFERRING EXPRESSION UNDERSTANDING TASK**

150 We define referring expression understanding as a unified framework for object recognition (either
 151 detection/segmentation) from referring expressions. Given an image I and a textual query q , a
 152 vision-language model (VLM) \mathcal{F} predicts one or more target objects, as formulated in Eq. 4:

$$\{O_1, \dots, O_N\} = \mathcal{F}(I, q), \quad (4)$$

153 where each O_i denotes a predicted object parsed from VLM text outputs, and N denotes the number
 154 of parsed objects. We define REC, Visual Grounding (VG) (Plummer et al., 2015), and Open-
 155 Vocabulary Detection (OVD) as instances of *Generalized REC* (GREC), where each referred object
 156 O_i is represented by a bounding box. Likewise, we define RES and Open-Vocabulary Segmen-
 157 tation (OVS) (Wu et al., 2024) as instances of *Generalized RES* (GRES), where each object O_i is
 158 represented by an instance mask.

159 In this work, we focus on three representative REU tasks: (i) REC, which targets single-object
 160 detection from complex reasoning queries; (ii) OVD, which addresses multi-object detection from

162 class-based queries; and (iii) GRES, which requires multi-object segmentation from complex reasoning queries. All tasks are studied under few-shot settings. In our formulation, each shot label
 163 refers to a annotated bounding box or mask. Specifically, in the GREC setup, one “shot” is defined
 164 as an image–query–box triplet, while in GRES, one “shot” corresponds to an image–query–mask
 165 triplet. Importantly, a ground-truth mask may include multiple valid instances for a single query
 166 (Li et al., 2025b). Among these tasks, GRES is the most challenging, as it requires the model to
 167 generate accurate segmentation masks for (multiple) objects described by natural-language queries
 168 in aerial images (Yuan et al., 2024).
 169

170 The few-shot setting substantially increases task difficulty by requiring models to generalize from
 171 only a handful of labeled examples, in contrast to large-scale datasets such as VRSBench (Li et al.,
 172 2024c) (36k training examples), and DIOR-RSVG (27k) (Zhan et al., 2023). Few-shot REU is
 173 particularly challenging due to: (1) *visual diversity*, arising from large variations in object size,
 174 orientation, appearance, and inter-object relationships; and (2) *description diversity*, as natural
 175 language queries may vary in structure, vocabulary, abstraction level, and reasoning complexity. These
 176 factors jointly make few-shot REU a more realistic yet significantly harder problem compared to
 177 conventional large-scale training scenarios.
 178

2.3 REWARD DESIGN

180 Following DeepSeek-R1, the reward function of Geo-R1 includes a task-agnostic format reward and
 181 a task-specific metrics reward. The format reward is applied uniformly across all tasks, whereas the
 182 metric reward is selected according to the requirements of each specific task.
 183

2.3.1 FORMAT REWARD

186 To ensure reliable parsing and evaluation, the model’s output must follow a well-defined
 187 structure. We define a binary format reward that checks whether the response conforms to
 188 this structure. The output must be wrapped in reasoning tags `<think>...</think>` and
 189 `<answer>...</answer>`. The format reward is defined as:

$$R_{\text{format}}(q, o) = \begin{cases} 1, & \text{if output follows the expected format} \\ 0, & \text{otherwise} \end{cases} \quad (5)$$

2.3.2 METRICS REWARD

195 **GREC.** For the REC task, the VLM predicts a single object bounding box, i.e., $b_{\text{pred}} = \mathcal{F}(I, q)$. An
 196 IoU reward can be calculated by comparing b_{pred} with the ground-truth box b_{gt} . For the OVD task,
 197 the VLM predicts is a set of box–label pairs, i.e., $\mathbb{B}_{\text{pred}} = \{(b_{\text{pred}}^i, c_{\text{pred}}^i)\}_{i=1}^N$, where b_{pred}^i denotes
 198 predicted bounding box, c_{pred}^i denotes category label. We then calculate reward as mAP¹ between
 199 \mathbb{B}_{pred} and corresponding ground truth \mathbb{B}_{gt} , along with a penalty coefficient for overlength predictions.
 200 The metrics reward for GREC task is defined as follow:

$$R_{\text{metrics}}(q, o) = \begin{cases} \text{IoU}(b_{\text{pred}}, b_{\text{gt}}), & \text{for REC task} \\ \min(1, \sqrt{\frac{N_{\text{gt}}}{N}}) \cdot \text{mAP}(\mathbb{B}_{\text{pred}}, \mathbb{B}_{\text{gt}}), & \text{for OVD task} \end{cases} \quad (6)$$

204 where N_{gt} denotes the number of ground truth objects.
 205

206 **GRES.** For GRES task, the VLM model is prompted to output a set of box–point pairs, $\mathbb{B}_{\text{pred}} =$
 207 $\{(b_{\text{pred}}^i, p_{\text{pred}}^i)\}_{i=1}^N$, where b_{pred}^i denotes a predicted bounding box and p_{pred}^i denotes the associated
 208 keypoints. These predictions are then provided as prompts to a frozen SAM to generate final instance
 209 masks \mathbb{M}_{pred} . Each predicted instance mask is trimmed to ensure its boundary does not exceed that
 210 of the corresponding bounding box. Finally, all instance masks are combined by taking their union
 211 to form a single predicted segmentation. Given ground truth instance masks \mathbb{M}_{gt} , the metrics reward
 212 for GRES task is defined as follows:
 213

$$R_{\text{metrics}}(q, o) = \text{MaskGIoU}(\mathbb{M}_{\text{pred}}, \mathbb{M}_{\text{gt}}). \quad (7)$$

214 We follow LISA (Lai et al., 2024) to calculate mask GIoU.
 215

¹We set the confidence score of all predicted bounding boxes to 1.

216

3 MAIN EXPERIMENT

217

3.1 EXPERIMENT SETUP

218 **Datasets.** Unlike conventional few-shot learning (e.g., Prototypical Networks (Snell et al., 2017)
 219 and TFA (Wang et al., 2020)), we do not partition the dataset into base and novel classes. Instead,
 220 we treat all classes as novel and provide only a few labeled examples per class. We construct
 221 instruction-following few-shot datasets for the GREC and GRES tasks by deriving them from the
 222 training sets of three widely used remote sensing benchmarks: VRSBench Li et al. (2024c), NWPU
 223 VHR-10 (Cheng et al., 2014), and EarthReason (Li et al., 2025b). Configurations and statistics are
 224 summarized in Table 1. *The term “shot” defines the number of samples per object category.* For
 225 the OVD task, we select four classes on which the baseline model (Qwen2.5-VL-3B) demonstrated
 226 decent performance. We select all categories from the training set for other tasks. The low-shot
 227 dataset is a subset of the high-shot dataset. To evaluate cross-dataset generalization, we further
 228 evaluate zero-shot performance on DIOR-RSVG (Zhan et al., 2023) and RRSIS-D (Yuan et al.,
 229 2024) datasets.
 230

231

Table 1: Overview of our Few-Shot Referring Expression Understanding Datasets.

Dataset Name	Source Dataset	Task	# Categories	# Shots	# VQAs	# Images	Shot Definition
VRSBench-FS	VRSBench	REC	26	{10, 5, 1}	260	254	image-query-box
NWPU-FS	NWPU VHR-10	OVD	4	{10, 5}	25	25	image-query-box
EarthReason-FS	EarthReason	GRES	24	{10, 5, 1}	240	240	image-query-mask

232 **Model and Training Details.** We adopt Qwen2.5-VL-3B-Instruct (Bai et al., 2025) as base model.
 233 Our implementation is built on the VLM-R1² and Easy-R1³ codebase. Unless otherwise specified,
 234 we strictly inherit the default hyperparameters without manual tuning. We set the same batch size for
 235 different post-training paradigm. We trained comparing models for 30 epochs, with early stopping
 236 when the reward converged. All experiments are conducted on 8 × H100 GPUs, and a full training
 237 run takes approximately 10 to 20 hours. Prompt templates are shown in Appendix C. We apply
 238 thinking prompts for RL-based Paradigms. We adopt GRPO as our primary RL-based post-training
 239 paradigm. For SFT-based post-training, we perform visual instruction tuning with standard next
 240 token prediction (NTP) loss, implemented via LLaMA-Factory (Zheng et al., 2024).
 241

242

3.2 FEW-SHOT GENERALIZED REFERRING EXPRESSION COMPREHENSION - REC

243 **Task Evaluation.** Performance on the REC subtask is measured by $\text{Acc}@\tau$ (a prediction is correct
 244 if its box IoU with the ground truth exceeds τ) in the test set of VRSBench. We report metrics for
 245 $\text{Acc}@0.5$ and $\text{Acc}@0.7$. The experiments are conducted in 1-shot, 5-shot, and 10-shot configura-
 246 tions, with “Unique,” “Non-Unique,” and overall results reported. This evaluation compares the SFT
 247 method against two RL-based approaches, GRPO (Shao et al., 2024) and DAPO (Yu et al., 2025).
 248 We highlight the performance gap in red.
 249

250 **Results.** Table 2 compares models trained on the full VRSBench (Full Amount Fine-tune) against
 251 few-shot models (1/5/10-shot Fine-tune). The few-shot results include both SFT-based models and
 252 our RL-tuned models. Performance data for the full-data baselines (except Qwen2.5-VL) are taken
 253 from the original VRSBench paper. The results reveal a clear performance hierarchy: RL-based
 254 post-training methods consistently and significantly outperform the SFT approach across all settings
 255 and metrics. This advantage is substantial; for example, in the 10-shot overall setting, our GRPO-
 256 based model achieves an $\text{Acc}@0.5$ score 12.30% higher than its SFT counterpart. Remarkably,
 257 our 10-shot GRPO model using only 260 samples, 0.71% data, achieves a score that surpasses all
 258 evaluated models (except Qwen2.5-VL) trained on all 36,313 samples.
 259

260 Within RL-based approaches, DAPO consistently outperforms GRPO across nearly all scenarios,
 261 indicating that more effective RL training could further enhance performance in few-shot settings.
 262 Moreover, the gains from RL-based methods are more pronounced on the Unique subset than on the
 263 Non-Unique subset, suggesting that RL approaches provide a larger boost on simpler tasks that do
 264 not require distinguishing between same-category distractors.
 265

²<https://github.com/om-ai-lab/VLM-R1>

³<https://github.com/hiyouga/EasyR1>

270 Table 2: Performance on VRSBench for the REC task. We report grounding accuracy at IoU thresh-
 271 olds of 0.5 and 0.7. Unique and Non-Unique indicate whether a referred object is the only instance
 272 of its category in the image or not.

273 274 Method	275 276 277 278 Base LLM	279 280 281 282 Unique		283 284 285 286 287 288 Non-Unique		289 290 291 292 293 294 Overall	
		295 296 297 298 Acc@0.5	299 300 301 302 Acc@0.7	303 304 305 306 Acc@0.5	307 308 309 310 Acc@0.7	311 312 313 314 Acc@0.5	315 316 317 318 Acc@0.7
279 280 281 282 Full Amount Fine-tune (36,313 samples)							
283 284 285 286 287 288 289 290 291 292 293 294 295 296 297 298 299 300 295 296 297 298 299 300 301 302 303 304 305 306 307 308 309 310 311 312 313 314 315 316 317 318 319 320 321 322 323 324 325 326 327 328 329 330 331 332 333 334 335 336 337 338 339 340 341 342 343 344 345 346 347 348 349 350 351 352 353 354 355 356 357 358 359 360 361 362 363 364 365 366 367 368 369 370 371 372 373 374 375 376 377 378 379 380 381 382 383 384 385 386 387 388 389 390 391 392 393 394 395 396 397 398 399 400 401 402 403 404 405 406 407 408 409 410 411 412 413 414 415 416 417 418 419 420 421 422 423 424 425 426 427 428 429 430 431 432 433 434 435 436 437 438 439 440 441 442 443 444 445 446 447 448 449 450 451 452 453 454 455 456 457 458 459 460 461 462 463 464 465 466 467 468 469 470 471 472 473 474 475 476 477 478 479 480 481 482 483 484 485 486 487 488 489 490 491 492 493 494 495 496 497 498 499 500 501 502 503 504 505 506 507 508 509 510 511 512 513 514 515 516 517 518 519 520 521 522 523 524 525 526 527 528 529 530 531 532 533 534 535 536 537 538 539 540 541 542 543 544 545 546 547 548 549 550 551 552 553 554 555 556 557 558 559 5510 5511 5512 5513 5514 5515 5516 5517 5518 5519 5520 5521 5522 5523 5524 5525 5526 5527 5528 5529 5530 5531 5532 5533 5534 5535 5536 5537 5538 5539 5540 5541 5542 5543 5544 5545 5546 5547 5548 5549 5550 5551 5552 5553 5554 5555 5556 5557 5558 5559 55510 55511 55512 55513 55514 55515 55516 55517 55518 55519 55520 55521 55522 55523 55524 55525 55526 55527 55528 55529 55530 55531 55532 55533 55534 55535 55536 55537 55538 55539 55540 55541 55542 55543 55544 55545 55546 55547 55548 55549 55550 55551 55552 55553 55554 55555 55556 55557 55558 55559 55560 55561 55562 55563 55564 55565 55566 55567 55568 55569 55570 55571 55572 55573 55574 55575 55576 55577 55578 55579 55580 55581 55582 55583 55584 55585 55586 55587 55588 55589 55590 55591 55592 55593 55594 55595 55596 55597 55598 55599 555100 555101 555102 555103 555104 555105 555106 555107 555108 555109 555110 555111 555112 555113 555114 555115 555116 555117 555118 555119 555120 555121 555122 555123 555124 555125 555126 555127 555128 555129 555130 555131 555132 555133 555134 555135 555136 555137 555138 555139 555140 555141 555142 555143 555144 555145 555146 555147 555148 555149 555150 555151 555152 555153 555154 555155 555156 555157 555158 555159 555160 555161 555162 555163 555164 555165 555166 555167 555168 555169 555170 555171 555172 555173 555174 555175 555176 555177 555178 555179 555180 555181 555182 555183 555184 555185 555186 555187 555188 555189 555190 555191 555192 555193 555194 555195 555196 555197 555198 555199 555200 555201 555202 555203 555204 555205 555206 555207 555208 555209 555210 555211 555212 555213 555214 555215 555216 555217 555218 555219 555220 555221 555222 555223 555224 555225 555226 555227 555228 555229 555230 555231 555232 555233 555234 555235 555236 555237 555238 555239 555240 555241 555242 555243 555244 555245 555246 555247 555248 555249 555250 555251 555252 555253 555254 555255 555256 555257 555258 555259 555260 555261 555262 555263 555264 555265 555266 555267 555268 555269 555270 555271 555272 555273 555274 555275 555276 555277 555278 555279 555280 555281 555282 555283 555284 555285 555286 555287 555288 555289 555290 555291 555292 555293 555294 555295 555296 555297 555298 555299 5552910 5552911 5552912 5552913 5552914 5552915 5552916 5552917 5552918 5552919 55529110 55529111 55529112 55529113 55529114 55529115 55529116 55529117 55529118 55529119 555291110 555291111 555291112 555291113 555291114 555291115 555291116 555291117 555291118 555291119 5552911110 5552911111 5552911112 5552911113 5552911114 5552911115 5552911116 5552911117 5552911118 5552911119 55529111110 55529111111 55529111112 55529111113 55529111114 55529111115 55529111116 55529111117 55529111118 55529111119 555291111110 555291111111 555291111112 555291111113 555291111114 555291111115 555291111116 555291111117 555291111118 555291111119 5552911111110 5552911111111 5552911111112 5552911111113 5552911111114 5552911111115 5552911111116 5552911111117 5552911111118 5552911111119 55529111111110 55529111111111 55529111111112 55529111111113 55529111111114 55529111111115 55529111111116 55529111111117 55529111111118 55529111111119 555291111111110 555291111111111 555291111111112 555291111111113 555291111111114 555291111111115 555291111111116 555291111111117 555291111111118 555291111111119 5552911111111110 5552911111111111 5552911111111112 5552911111111113 5552911111111114 5552911111111115 5552911111111116 5552911111111117 5552911111111118 5552911111111119 55529111111111110 55529111111111111 55529111111111112 55529111111111113 55529111111111114 55529111111111115 55529111111111116 55529111111111117 55529111111111118 55529111111111119 555291111111111110 555291111111111111 555291111111111112 555291111111111113 555291111111111114 555291111111111115 555291111111111116 555291111111111117 555291111111111118 555291111111111119 5552911111111111110 5552911111111111111 5552911111111111112 5552911111111111113 5552911111111111114 5552911111111111115 5552911111111111116 5552911111111111117 5552911111111111118 5552911111111111119 55529111111111111110 55529111111111111111 55529111111111111112 55529111111111111113 55529111111111111114 55529111111111111115 55529111111111111116 55529111111111111117 55529111111111111118 55529111111111111119 555291111111111111110 5552911111111111111111 5552911111111111111112 5552911111111111111113 5552911111111111111114 5552911111111111111115 5552911111111111111116 5552911111111111111117 5552911111111111111118 5552911111111111111119 55529111111111111111110 555291111111111111111111 555291111111111111111112 555291111111111111111113 555291111111111111111114 555291111111111111111115 555291111111111111111116 555291111111111111111117 555291111111111111111118 555291111111111111111119 5552911111111111111111110 5552911111111111111111111 5552911111111111111111112 5552911111111111111111113 5552911111111111111111114 5552911111111111111111115 5552911111111111111111116 5552911111111111111111117 5552911111111111111111118 5552911111111111111111119 55529111111111111111111110 55529111111111111111111111 55529111111111111111111112 55529111111111111111111113 55529111111111111111111114 55529111111111111111111115 55529111111111111111111116 55529111111111111111111117 55529111111111111111111118 55529111111111111111111119 555291111111111111111111110 555291111111111111111111111 555291111111111111111111112 555291111111111111111111113 555291111111111111111111114 555291111111111111111111115 555291111111111111111111116 555291111111111111111111117 555291111111111111111111118 555291111111111111111111119 5552911111111111111111111110 5552911111111111111111111111 5552911111111111111111111112 5552911111111111111111111113 5552911111111111111111111114 5552911111111111111111111115 5552911111111111111111111116 5552911111111111111111111117 5552911111111111111111111118 5552911111111111111111111119 55529111111111111111111111110 55529111111111111111111111111 55529111111111111111111111112 55529111111111111111111111113 55529111111111111111111111114 55529111111111111111111111115 55529111111111111111111111116 55529111111111111111111111117 55529111111111111111111111118 55529111111111111111111111119 555291111111111111111111111110 555291111111111111111111111111 555291111111111111111111111112 555291111111111111111111111113 555291111111111111111111111114 555291111111111111111111111115 555291111111111111111111111116 555291111111111111111111111117 555291111111111111111111111118 555291111111111111111111111119 5552911111111111111111111111110 5552911111111111111111111111111 5552911111111111111111111111112 5552911111111111111111111111113 5552911111111111111111111111114 5552911111111111111111111111115 5552911111111111111111111111116 5552911111111111111111111111117 5552911111111111111111111111118 5552911111111111111111111111119 55529111111111111111111111111110 55529111111111111111111111111111 555291111111111111111111111111112 555291111111111111111111111111113 555291111111111111111111111111114 555291111111111111111111111111115 555291111111111111111111111111116 555291111111111111111111111111117 555291111111111111111111111111118 555291111111111111111111111111119 5552911111111111111111111111111110 5552911111111111111111111111111111 55529111111111111111111111111111112 55529111111111111111111111111111113 55529111111111111111111111111111114 55529111111111111111111111111111115 55529111111111111111111111111111116 55529111111111111111111111111111117 55529111111111111111111111111111118 55529111111111111111111111111111119 555291111111111111111111111111111110 555291111111111111111111111111111111 555291111111111111111111111111111112 555291111111111111111111111111111113 555291111111111111111111111111111114 555291111111111111111111111111111115 555291111111111111111111111111111116 555291111111111111111111111111111117 555291111111111111111111111111111118 555291111111111111111111111111111119 5552911111111111111111111111111111110 5552911111111111111111111111111111111 5552911111111111111111111111111111112 5552911111111111111111111111111111113 5552911111111111111111111111111111114 5552911111111111111111111111111111115 5552911111111111111111111111111111116 5552911111111111111111111111111111117 555291111111							

324 by the mask-based gIoU, defined by the average of all per-image IoUs. We use this metric because
 325 alternatives like cloU are highly biased toward large-area objects and tend to fluctuate significantly.
 326 We report the final gIoU scores on the validation and test sets of the EarthReason dataset. To ensure a
 327 fair comparison with SFT-based approaches, we evaluate our method against SegEarth-R1 (Li et al.,
 328 2025b), trained on the same dataset. SegEarth-R1 serves as a strong SFT baseline, as it employs an
 329 auxiliary segmentation decoder to generate pixel-level masks through a differentiable mask loss.

330 **Results.** In Table 4, we demonstrate the effective results of our proposed
 331 pipeline and task-specific reward for training reasoning models on GRES task.
 332 First, we found our GRPO-trained model, i.e., Geo-
 333 R1, demonstrates a significant improvement com-
 334 pared to the zero-shot baseline. It achieves a gIoU
 335 increase of up to 38.48% on the validation set (from
 336 19.35% to 57.78%) and up to 26.11% on the test set
 337 (from 32.16% to 58.27%), showing the success of
 338 RL-based post-training paradigm. Then, we observe
 339 that the model exhibits remarkable performance with
 340 a very small number of samples. With just 240 sam-
 341 ples (10-shot), our model demonstrates a compara-
 342 ble performance with PixelLM, which are trained
 343 on 900K instances with descriptions. *Using only*
 344 *240 samples (10-shot), which is roughly 2% train-
 345 ing data, Geo-R1 reaches nearly 83% of the per-
 346 formance of the SegEarth-R1 model that was trained on
 347 the entire training set.*

348 In a direct comparison, the GRPO pipeline consis-
 349 tently yields superior models to the SFT approach.
 350 Geo-R1 outperforms SegEarth-R1 in both the 10-
 351 shot and 5-shot settings. Crucially, *this performance*
 352 *gap becomes more significant as the amount of train-
 353 ing data decreases*. This trend indicates that RL-
 354 based post-training paradigm is a more effective and
 355 sample-efficient method for adapting large VLM to
 356 this specialized, pixel-level task, especially in data-
 357 scarce scenarios.

358 4 DISCUSSION

361 In this section, we first compare the learning dynamics of SFT and GRPO, then examine cross-
 362 dataset generalization, the upper bound of few-shot learning, and the impact of model size. Unless
 363 otherwise specified, experiments are conducted on the VRSBench-FS dataset under the 10-shot
 364 setting.

366 4.1 LEARNING CURVE COMPARISON

368 We fine-tune Qwen2.5-VL-3B with both SFT and
 369 GRPO on the REC task using same batch size and
 370 evaluate checkpoints every 100 steps to sketch the
 371 learning curve. As shown in Figure 2, GRPO con-
 372 stantly outperforms SFT at every checkpoint, with
 373 an average gain of 9.74%. GRPO improves steadily,
 374 peaking around 400 steps, and remains strong until
 375 the end, whereas SFT oscillated within 37%–40%.
 376 GRPO achieves a clearly higher ceiling and sta-
 377 bilizes around 50%, indicating better training effi-
 378 ciency under few-shot setting.

Table 4: Performance on the EarthReason for the GRES task. We report gIoU.

	Val	Test
Full Amount Fine-tune		
LISA	61.04	60.88
PixelLM	57.94	60.01
PSALM	66.61	68.30
SegEarth-R1	68.60	70.75
Zero-shot Baseline		
Qwen2.5-VL w/ thinking	19.35	32.16
1-shot Fine-tune (24 samples)		
SegEarth-R1	42.47	43.01
Geo-R1	51.38	50.30
5-shot Fine-tune (120 samples)		
SegEarth-R1	45.37	45.46
Geo-R1	54.73	56.01
10-shot Fine-tune (240 samples)		
SegEarth-R1	56.40	56.60
Geo-R1	57.78	58.27

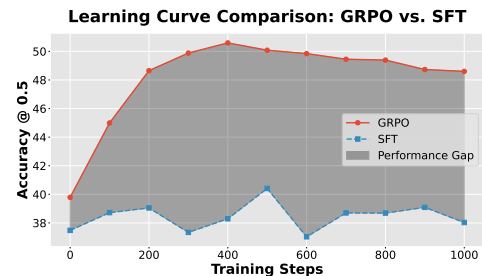


Figure 2: Learning curves of GRPO vs. SFT on REC.

378
379

4.2 CROSS DATASET GENERALIZATION

380
381
382
383
384
385
386
387
388
389

We further assess the cross-dataset generalization of the SFT and GRPO approaches on the GREC and GRES tasks. For the GREC task, we fine-tune models on the VRSBench dataset with limited supervision (1, 5, and 10-shot) and then evaluate model performance on the DIOR-RSVG target dataset, in a zero-shot manner. As shown in Table 5, GRPO consistently outperforms SFT across all settings, achieving a performance advantage of 4.92%, 6.05%, and 5.52% in the 1-shot, 5-shot, and 10-shot scenarios, respectively.

390
391
392
393
394

Similarly, for the GRES task, models were tuned on the EarthReason dataset (1, 5, and 10-shot) and tested on the RRSIS-D dataset. Here, the GRPO-based model (Geo-R1) demonstrates a remarkable improvement over the SFT-based model (SegEarth-R1) under few-shot setting, achieving a relative improvement up to 80%. These results highlight GRPO’s incredible cross-dataset generalization, indicating superior transferability and robustness of Geo-R1.

395
396

4.3 UPPER BOUND OF FEW-SHOT LEARNING

397
398
399
400
401
402
403
404
405
406
407
408
409
410

As shown in Figure 3, GRPO clearly outperforms SFT in low-shot settings, although this performance gap narrows as supervision increases. To investigate this trend and determine the upper-bound capability of Geo-R1, we experimented with additional shot numbers (20, 50, 100, and 200). Concretely, the margin between GRPO and SFT approaches shrinks from 13.03% at 1-shot to 0.47% at 200-shot. This diminishing advantage suggests both approaches approach a common upper bound with more data. Empirically, they converge toward the full-data SFT result of 62.91%, indicating GRPO’s strong sample efficiency at small shots but similar asymptotic performance as shot count grows.

411
412

4.4 FEW-SHOT LEARNING MEETS MODEL SIZE

413
414
415
416
417
418
419
420
421
422
423
424
425
426
427
428
429

We then examine how model size influences the performance under different post-training paradigms. As shown in Figure 4, both SFT and GRPO benefit from increased model scales. However, this trend exhibits clear diminishing marginal returns. For instance, SFT gains 4.31% when scaling from 3B to 7B but only 2.23% from 7B to 32B, with a similar slowdown observed for GRPO from 3B to 7B. This suggests that while larger models provide a stronger foundation, simply increasing number of parameters yields limited benefits for the few-shot task. This can be attributed to the limited fine-tuning data. With few examples, high-capacity models tend to overfit by simply memorizing the training samples rather than learning generalizable features. Notably, GRPO’s performance decreased on the 32B model, likely due to two factors: overfitting on limited data and numerical instability from bf16 training.

5 RELATED WORK

430
431

Reasoning LLMs and VLMs. The OpenAI o1 (Jaech et al., 2024) showed that RL improves the reasoning capability of LLMs by learning from feedback on final outcomes. Recently, DeepSeek-

# shot	VRSBench → DIOR-RSVG		EarthReason → RRSIS-D	
	SegEarth-R1	Geo-R1	SegEarth-R1	Geo-R1
1-shot	32.35	37.27 (4.92)	18.77	32.11 (13.54)
5-shot	34.52	40.57 (6.05)	20.29	36.41 (16.12)
10-shot	34.86	40.38 (5.52)	24.27	37.83 (13.56)

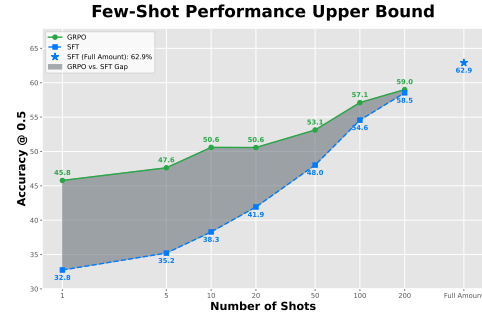


Figure 3: Few-shot Learning Upper-Bound.

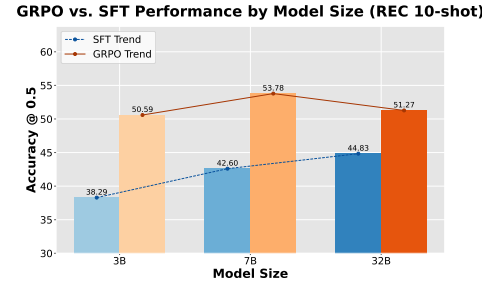


Figure 4: Few-shot Learning Meets Model Size.

R1 (Guo et al., 2025) demonstrated that rule-based rewards can be used with the GRPO algorithm to teach LLMs advanced reasoning skills. Inspired by the success of RL in LLMs, researchers are now applying the R1 framework to VLMs. R1-OneVision (Yang et al., 2025) created a step-by-step multimodal reasoning datasets for SFT and RL. Concurrently, R1-V (Chen et al., 2025) applied the GRPO algorithm to object counting, achieving the remarkable result of a 3B model outperforming much larger 72B models. VisualThinker-R1-Zero (Zhou et al., 2025) applied it directly to base VLMs, observing “visual aha moments”. Other studies refined the training process: Vision-R1 (Huang et al., 2025) first created a multimodal CoT dataset, serving as a cold-start before RL; LMM-R1 (Peng et al., 2025) used a two-phase strategy, starting with text-only reasoning before fine-tuning on multimodal data. Visual-RFT (Liu et al., 2025b), VLM-R1 (Shen et al., 2025), and Seg-Zero (Liu et al., 2025a) explored applying RL to image perception tasks.

Few-shot Learning in Remote Sensing. Few-shot learning (FSL) is crucial in RS, since it effectively addresses the challenge of limited labeled data. Attention-based contrastive learning have been shown to significantly improve classification accuracy in scene classification tasks (Xu et al., 2024; Zeng & Geng, 2022). Prototype-based networks (Li et al., 2021; Cheng et al., 2022) and multi-scale feature fusion strategies (Zhao et al., 2022) help models obtain diverse object characteristics, achieving state-of-the-art results on RS object detection benchmarks under few-shot settings. For segmentation, adaptive prototype clustering and mask-guided correlation learning enable precise pixel-level interpretation even with few annotated samples (Jiang et al., 2022; Jia et al., 2025; Li et al., 2024b; Shen et al., 2024). FSL enhances the efficiency and interpretability of RSI analysis, while also addressing key challenges in generalization and multimodal integration (Sun et al., 2021; Lee et al., 2024).

REC and RES in Remote Sensing. Referring expression comprehension in remote sensing—often termed remote sensing visual grounding (RSVG), which localizes a target in aerial imagery from a natural-language description. Early progress was established by the RSVG benchmark and the GeoVG model (Sun et al., 2022), and extended by DIOR-RSVG to broaden categories and scene scale (Zhan et al., 2023). In the MLLM era, GeoChat (Kuckreja et al., 2024) was the first MLLM to handle a wide range of RS vision-language tasks, including RSVG. Later, VRSBench (Li et al., 2024c) provided a high-quality dataset for RSVG task. RS-specific MLLMs such as EarthGPT (Zhang et al., 2024), RSGPT (Hu et al., 2025), SkySenseGPT (Luo et al., 2024), VHM (Pang et al., 2025), further unified different vision-language tasks, such as captioning, VG, VQA, and OVD, thus improving RS-specific alignment. For RES, Yuan et al. introduced the RES task for RS and released the RefSegRS dataset (Yuan et al., 2024). Liu et al. later introduced RRSIS-D, enabling pixel-level referring at scale (Liu et al., 2024d). Recent works such as GeoGround (Zhou et al., 2024b) and Skysense-O (Zhu et al., 2025) further unified the REC and RES tasks for RS images. Besides, works for OVD (Li et al., 2024e; Pan et al., 2025), and OVS (Li et al., 2025a;b) can be viewed as a special case of REC and RES (locate multiple objects with template-based description), which support grounding of novel categories.

6 CONCLUSION

In this work, we define a generic task, Referring Expression Understanding that aims to recognize objects (either detection/segmentation) from referring expressions. We then compare RL-based (GRPO) and SFT-based post-training paradigms on few-shot REC, OVD, and GRES tasks within the RS domain. Our results show that our GRPO-trained model, Geo-R1, consistently outperforms standard SFT-tuned models across these tasks. The performance gains are particularly large in low-shot regimes, and the model exhibits significantly stronger cross-dataset generalization.

While our study demonstrates the effectiveness of reinforcement learning for few-shot referring expression understanding, several avenues remain. Our evaluation is limited to high-resolution aerial imagery; extending Geo-R1 to multispectral (e.g., Sentinel-2) and SAR data would further test its robustness. Beyond the three REU tasks studied (REC, RES, OVD), future work could explore broader grounding tasks, e.g., OVS. Finally, scaling to larger shots, refining reward functions, and designing powerful RL training recipes remain promising directions.

486 REFERENCES
487

488 Shuai Bai, Keqin Chen, Xuejing Liu, Jialin Wang, Wenbin Ge, Sibo Song, Kai Dang, Peng Wang,
489 Shijie Wang, Jun Tang, Humen Zhong, Yuanzhi Zhu, Mingkun Yang, Zhaohai Li, Jianqiang Wan,
490 Pengfei Wang, Wei Ding, Zheren Fu, Yiheng Xu, Jiabo Ye, Xi Zhang, Tianbao Xie, Zesen Cheng,
491 Hang Zhang, Zhibo Yang, Haiyang Xu, and Junyang Lin. Qwen2.5-v1 technical report. *arXiv*
492 preprint *arXiv:2502.13923*, 2025.

493 Jun Chen, Deyao Zhu, Xiaoqian Shen, Xiang Li, Zechun Liu, Pengchuan Zhang, Raghuraman
494 Krishnamoorthi, Vikas Chandra, Yunyang Xiong, and Mohamed Elhoseiny. Minigpt-v2: large
495 language model as a unified interface for vision-language multi-task learning. *arXiv preprint*
496 *arXiv:2310.09478*, 2023.

497 Liang Chen, Lei Li, Haozhe Zhao, Yifan Song, and Vinci. R1-v: Reinforcing super generalization
498 ability in vision-language models with less than \$3. <https://github.com/Deep-Agent/R1-V>, 2025. Accessed: 2025-02-02.

499 500 Gong Cheng, Junwei Han, Peicheng Zhou, and Lei Guo. Multi-class geospatial object detection
501 and geographic image classification based on collection of part detectors. *ISPRS Journal of Photo-*
502 *grammetry and Remote Sensing*, 98:119–132, 2014.

503 504 Gong Cheng, Bowei Yan, Peizhen Shi, Ke Li, Xiwen Yao, Lei Guo, and Junwei Han. Prototype-cnn
505 for few-shot object detection in remote sensing images. *IEEE Transactions on Geoscience and*
506 *Remote Sensing*, 60:1–10, 2022. doi: 10.1109/TGRS.2021.3078507.

507 508 Daya Guo, Dejian Yang, Haowei Zhang, Junxiao Song, Peiyi Wang, Qihao Zhu, Runxin Xu, Ruoyu
509 Zhang, Shirong Ma, Xiao Bi, et al. Deepseek-r1 incentivizes reasoning in llms through reinforce-
510 ment learning. *Nature*, 645(8081):633–638, 2025.

511 512 Yuan Hu, Jianlong Yuan, Congcong Wen, Xiaonan Lu, Yu Liu, and Xiang Li. Rsgpt: A remote
513 sensing vision language model and benchmark. *ISPRS Journal of Photogrammetry and Remote*
514 *Sensing*, 224:272–286, 2025.

515 516 Wenxuan Huang, Bohan Jia, Zijie Zhai, Shaosheng Cao, Zheyu Ye, Fei Zhao, Yao Hu, and Shaohui
517 Lin. Vision-r1: Incentivizing reasoning capability in multimodal large language models. *arXiv*
518 preprint *arXiv:2503.06749*, 2025.

519 520 Aaron Jaech, Adam Kalai, Adam Lerer, Adam Richardson, Ahmed El-Kishky, Aiden Low, Alec
521 Helyar, Aleksander Madry, Alex Beutel, Alex Carney, et al. Openai o1 system card. *arXiv*
522 preprint *arXiv:2412.16720*, 2024.

523 524 Yuyu Jia, Jiabo Li, and Qi Wang. Generalized few-shot semantic segmentation for remote sensing
525 images. *IEEE Transactions on Geoscience and Remote Sensing*, 63:1–10, 2025. doi: 10.1109/
526 TGRS.2025.3531874.

527 528 Xufeng Jiang, Nan Zhou, and Xiang Li. Few-shot segmentation of remote sensing images using
529 deep metric learning. *IEEE Geoscience and Remote Sensing Letters*, 19:1–5, 2022.

530 531 Kartik Kuckreja, Muhammad S Danish, Muzammal Naseer, Abhijit Das, Salman Khan, and Fahad S
532 Khan. Geochat: Grounded large vision-language model for remote sensing. the ieee. In *CVF*
533 *Conference on Computer Vision and Pattern Recognition*, volume 2, pp. 4, 2024.

534 535 Xin Lai, Zhuotao Tian, Yukang Chen, Yanwei Li, Yuhui Yuan, Shu Liu, and Jiaya Jia. Lisa: Rea-
536 soning segmentation via large language model. In *Proceedings of the IEEE/CVF Conference on*
537 *Computer Vision and Pattern Recognition (CVPR)*, pp. 9579–9589, June 2024.

538 539 Gao Yu Lee, Tanmoy Dam, Md Meftahul Ferdaus, Daniel Puiu Poenar, and Vu N Duong. Unlocking
540 the capabilities of explainable few-shot learning in remote sensing. *Artificial Intelligence Review*,
541 57(7):169, 2024.

542 543 Kaiyu Li, Ruixun Liu, Xiangyong Cao, Xueru Bai, Feng Zhou, Deyu Meng, and Zhi Wang.
544 Segearth-ov: Towards training-free open-vocabulary segmentation for remote sensing images.
545 In *Proceedings of the Computer Vision and Pattern Recognition Conference*, pp. 10545–10556,
546 2025a.

540 Kaiyu Li, Zepeng Xin, Li Pang, Chao Pang, Yupeng Deng, Jing Yao, Guisong Xia, Deyu Meng, Zhi
 541 Wang, and Xiangyong Cao. Segearth-r1: Geospatial pixel reasoning via large language model.
 542 *arXiv preprint arXiv:2504.09644*, 2025b.

543 Ke Li, Di Wang, Haojie Xu, Haodi Zhong, and Cong Wang. Language-guided progressive attention
 544 for visual grounding in remote sensing images. *IEEE Transactions on Geoscience and Remote
 545 Sensing*, 62:1–13, 2024a. doi: 10.1109/TGRS.2024.3423663.

546 Shuo Li, Fang Liu, Licheng Jiao, Xu Liu, Puhua Chen, and Lingling Li. Mask-guided correlation
 547 learning for few-shot segmentation in remote sensing imagery. *IEEE Transactions on Geoscience
 548 and Remote Sensing*, 62:1–14, 2024b. doi: 10.1109/TGRS.2024.3417965.

549 Xiang Li, Jingyu Deng, and Yi Fang. Few-shot object detection on remote sensing images. *IEEE
 550 Transactions on Geoscience and Remote Sensing*, 60:1–14, 2021.

551 Xiang Li, Congcong Wen, Yuan Hu, and Nan Zhou. Rs-clip: Zero shot remote sensing scene
 552 classification via contrastive vision-language supervision. *International Journal of Applied Earth
 553 Observation and Geoinformation*, 124:103497, 2023.

554 Xiang Li, Jian Ding, and Mohamed Elhoseiny. Vrsbench: A versatile vision-language benchmark
 555 dataset for remote sensing image understanding. *Advances in Neural Information Processing
 556 Systems*, 37:3229–3242, 2024c.

557 Xiang Li, Congcong Wen, Yuan Hu, Zhenghang Yuan, and Xiao Xiang Zhu. Vision-language mod-
 558 els in remote sensing: Current progress and future trends. *IEEE Geoscience and Remote Sensing
 559 Magazine*, 12(2):32–66, 2024d.

560 Yan Li, Weiwei Guo, Xue Yang, Ning Liao, Dunyun He, Jiaqi Zhou, and Wenxian Yu. Toward
 561 open vocabulary aerial object detection with clip-activated student-teacher learning. In *European
 562 Conference on Computer Vision*, pp. 431–448. Springer, 2024e.

563 Yanwei Li, Yuechen Zhang, Chengyao Wang, Zhisheng Zhong, Yixin Chen, Ruihang Chu, Shaoteng
 564 Liu, and Jiaya Jia. Mini-gemini: Mining the potential of multi-modality vision language models.
 565 *arXiv preprint arXiv:2403.18814*, 2024f.

566 Fan Liu, Delong Chen, Zhangqinyun Guan, Xiaocong Zhou, Jiale Zhu, Qiaolin Ye, Liyong Fu,
 567 and Jun Zhou. Remoteclip: A vision language foundation model for remote sensing. *IEEE
 568 Transactions on Geoscience and Remote Sensing*, 62:1–16, 2024a.

569 Haotian Liu, Chunyuan Li, Yuheng Li, and Yong Jae Lee. Improved baselines with visual instruction
 570 tuning. In *2024 IEEE/CVF Conference on Computer Vision and Pattern Recognition (CVPR)*, pp.
 571 26286–26296, 2024b.

572 Shilong Liu, Zhaoyang Zeng, Tianhe Ren, Feng Li, Hao Zhang, Jie Yang, Qing Jiang, Chunyuan Li,
 573 Jianwei Yang, Hang Su, Jun Zhu, and Lei Zhang. Grounding dino: Marrying dino with grounded
 574 pre-training for open-set object detection, 2024c. URL <https://arxiv.org/abs/2303.05499>.

575 Sihan Liu, Yiwei Ma, Xiaoqing Zhang, Haowei Wang, Jiayi Ji, Xiaoshuai Sun, and Rongrong Ji.
 576 Rotated multi-scale interaction network for referring remote sensing image segmentation. In *2024
 577 IEEE/CVF Conference on Computer Vision and Pattern Recognition (CVPR)*, pp. 26648–26658,
 578 2024d.

579 Yuqi Liu, Bohao Peng, Zhisheng Zhong, Zihao Yue, Fanbin Lu, Bei Yu, and Jiaya Jia. Seg-
 580 zero: Reasoning-chain guided segmentation via cognitive reinforcement. *arXiv preprint
 581 arXiv:2503.06520*, 2025a.

582 Ziyu Liu, Zeyi Sun, Yuhang Zang, Xiaoyi Dong, Yuhang Cao, Haodong Duan, Dahua Lin, and Jiaqi
 583 Wang. Visual-rft: Visual reinforcement fine-tuning. *arXiv preprint arXiv:2503.01785*, 2025b.

584 Junwei Luo, Zhen Pang, Yongjun Zhang, Tingzhu Wang, Linlin Wang, Bo Dang, Jiangwei Lao, Jian
 585 Wang, Jingdong Chen, Yihua Tan, et al. Skysensegpt: A fine-grained instruction tuning dataset
 586 and model for remote sensing vision-language understanding. *arXiv preprint arXiv:2406.10100*,
 587 2024.

594 OpenAI. Gpt-4v(ision) system card. https://cdn.openai.com/papers/GPTV_System_Card.pdf, 2024. Accessed: 2025-08-30.

595

596

597 Jiancheng Pan, Yanxing Liu, Yuqian Fu, Muyuan Ma, Jiahao Li, Danda Pani Paudel, Luc Van Gool,

598 and Xiaomeng Huang. Locate anything on earth: Advancing open-vocabulary object detection

599 for remote sensing community. In *Proceedings of the AAAI Conference on Artificial Intelligence*,

600 volume 39, pp. 6281–6289, 2025.

601 Chao Pang, Xingxing Weng, Jiang Wu, Jiayu Li, Yi Liu, Jiaxing Sun, Weijia Li, Shuai Wang, Litong

602 Feng, Gui-Song Xia, et al. Vhm: Versatile and honest vision language model for remote sensing

603 image analysis. In *Proceedings of the AAAI Conference on Artificial Intelligence*, volume 39, pp.

604 6381–6388, 2025.

605 Yingzhe Peng, Gongrui Zhang, Miaozen Zhang, Zhiyuan You, Jie Liu, Qipeng Zhu, Kai Yang,

606 Xingzhong Xu, Xin Geng, and Xu Yang. Lmm-r1: Empowering 3b lmms with strong reasoning

607 abilities through two-stage rule-based rl. *arXiv preprint arXiv:2503.07536*, 2025.

608

609 Bryan A. Plummer, Liwei Wang, Chris M. Cervantes, Juan C. Caicedo, Julia Hockenmaier, and

610 Svetlana Lazebnik. Flickr30k entities: Collecting region-to-phrase correspondences for richer

611 image-to-sentence models. In *2015 IEEE International Conference on Computer Vision (ICCV)*,

612 pp. 2641–2649, 2015. doi: 10.1109/ICCV.2015.303.

613 Alec Radford, Jong Wook Kim, Chris Hallacy, Aditya Ramesh, Gabriel Goh, Sandhini Agarwal,

614 Girish Sastry, Amanda Askell, Pamela Mishkin, Jack Clark, et al. Learning transferable visual

615 models from natural language supervision. In *International conference on machine learning*, pp.

616 8748–8763. PmLR, 2021.

617 Nikhila Ravi, Valentin Gabeur, Yuan-Ting Hu, Ronghang Hu, Chaitanya Ryali, Tengyu Ma, Haitham

618 Khedr, Roman Rädle, Chloe Rolland, Laura Gustafson, Eric Mintun, Junting Pan, Kalyan Va-

619 sudev Alwala, Nicolas Carion, Chao-Yuan Wu, Ross Girshick, Piotr Dollar, and Christoph Fe-

620 ichtenhofer. SAM 2: Segment anything in images and videos. In *The Thirteenth International*

621 *Conference on Learning Representations*, 2025.

622 Zhihong Shao, Peiyi Wang, Qihao Zhu, Runxin Xu, Junxiao Song, Xiao Bi, Haowei Zhang,

623 Mingchuan Zhang, YK Li, Yang Wu, et al. Deepseekmath: Pushing the limits of mathemati-

624 cal reasoning in open language models. *arXiv preprint arXiv:2402.03300*, 2024.

625

626 Haozhan Shen, Peng Liu, Jingcheng Li, Chunxin Fang, Yibo Ma, Jiajia Liao, Qiaoli Shen, Zilun

627 Zhang, Kangjia Zhao, Qianqian Zhang, et al. Vlm-r1: A stable and generalizable r1-style large

628 vision-language model. *arXiv preprint arXiv:2504.07615*, 2025.

629 Weihao Shen, Ailong Ma, Junjue Wang, Zhuo Zheng, and Yanfei Zhong. Adaptive self-supporting

630 prototype learning for remote sensing few-shot semantic segmentation. *IEEE Transactions on*

631 *Geoscience and Remote Sensing*, 62:1–16, 2024. doi: 10.1109/TGRS.2024.3435086.

632 Jake Snell, Kevin Swersky, and Richard Zemel. Prototypical networks for few-shot learning. *Ad-*

633 *vances in neural information processing systems*, 30, 2017.

634

635 Xian Sun, Bing Wang, Zhirui Wang, Hao Li, Hengchao Li, and Kun Fu. Research progress on

636 few-shot learning for remote sensing image interpretation. *IEEE Journal of Selected Topics in*

637 *Applied Earth Observations and Remote Sensing*, 14:2387–2402, 2021. doi: 10.1109/JSTARS.

638 2021.3052869.

639 Yuxi Sun, Shanshan Feng, Xutao Li, Yunming Ye, Jian Kang, and Xu Huang. Visual grounding in

640 remote sensing images. In *Proceedings of the 30th ACM International Conference on Multimedia*,

641 MM '22, pp. 404–412, New York, NY, USA, 2022. Association for Computing Machinery. ISBN

642 9781450392037. doi: 10.1145/3503161.3548316.

643 Xin Wang, Thomas Huang, Joseph Gonzalez, Trevor Darrell, and Fisher Yu. Frustratingly simple

644 few-shot object detection. In *International Conference on Machine Learning*, pp. 9919–9928.

645 PMLR, 2020.

646

647 Xingxing Weng, Chao Pang, and Gui-Song Xia. Vision-language modeling meets remote sensing:

Models, datasets, and perspectives. *IEEE Geoscience and Remote Sensing Magazine*, 2025.

648 Jianzong Wu, Xiangtai Li, Shilin Xu, Haobo Yuan, Henghui Ding, Yibo Yang, Xia Li, Jiangning
 649 Zhang, Yunhai Tong, Xudong Jiang, et al. Towards open vocabulary learning: A survey. *IEEE*
 650 *Transactions on Pattern Analysis and Machine Intelligence*, 46(7):5092–5113, 2024.

651

652 Yulong Xu, Hanbo Bi, Hongfeng Yu, Wanxuan Lu, Peifeng Li, Xinming Li, and Xian Sun.
 653 Attention-based contrastive learning for few-shot remote sensing image classification. *IEEE*
 654 *Transactions on Geoscience and Remote Sensing*, 62:1–17, 2024. doi: 10.1109/TGRS.2024.
 655 3385655.

656

657 Yi Yang, Xiaoxuan He, Hongkun Pan, Xiyan Jiang, Yan Deng, Xingtao Yang, Haoyu Lu, Dacheng
 658 Yin, Fengyun Rao, Minfeng Zhu, et al. R1-onevision: Advancing generalized multimodal rea-
 659 soning through cross-modal formalization. *arXiv preprint arXiv:2503.10615*, 2025.

660

661 Qiyi Yu, Zheng Zhang, Ruofei Zhu, Yufeng Yuan, Xiaochen Zuo, Yu Yue, Weinan Dai, Tiantian
 662 Fan, Gaohong Liu, Lingjun Liu, et al. Dapo: An open-source llm reinforcement learning system
 663 at scale. *arXiv preprint arXiv:2503.14476*, 2025.

664

665 Zhenghang Yuan, Lichao Mou, Yuansheng Hua, and Xiao Xiang Zhu. Rrsis: Referring remote
 666 sensing image segmentation. *IEEE Transactions on Geoscience and Remote Sensing*, 2024.

667

668 Qingjie Zeng and Jie Geng. Task-specific contrastive learning for few-shot remote sensing image
 669 scene classification. *ISPRS Journal of Photogrammetry and Remote Sensing*, 191:143–154, 2022.

670

671 Yang Zhan, Zhitong Xiong, and Yuan Yuan. Rsvg: Exploring data and models for visual grounding
 672 on remote sensing data. *IEEE Transactions on Geoscience and Remote Sensing*, 61:1–13, 2023.

673

674 Wei Zhang, Miaoxin Cai, Tong Zhang, Yin Zhuang, and Xuerui Mao. Earthgpt: A universal mul-
 675 timodal large language model for multisensor image comprehension in remote sensing domain.
 676 *IEEE Transactions on Geoscience and Remote Sensing*, 62:1–20, 2024.

677

678 Zhitao Zhao, Ping Tang, Lijun Zhao, and Zheng Zhang. Few-shot object detection of remote sensing
 679 images via two-stage fine-tuning. *IEEE Geoscience and Remote Sensing Letters*, 19:1–5, 2022.
 680 doi: 10.1109/LGRS.2021.3116858.

681

682 Yaowei Zheng, Richong Zhang, Junhao Zhang, Yanhan Ye, Zheyuan Luo, Zhangchi Feng, and
 683 Yongqiang Ma. Llamafactory: Unified efficient fine-tuning of 100+ language models. *arXiv*
 684 *preprint arXiv:2403.13372*, 2024.

685

686 Hengguang Zhou, Xirui Li, Ruochen Wang, Minhao Cheng, Tianyi Zhou, and Cho-Jui Hsieh. R1-
 687 zero’s “aha moment” in visual reasoning on a 2b non-sft model. *arXiv preprint arXiv:2503.05132*,
 688 2025.

689

690 Yue Zhou, Litong Feng, Yiping Ke, Xue Jiang, Junchi Yan, Xue Yang, and Wayne Zhang. Towards
 691 vision-language geo-foundation model: A survey. *arXiv preprint arXiv:2406.09385*, 2024a.

692

693 Yue Zhou, Mengcheng Lan, Xiang Li, Litong Feng, Yiping Ke, Xue Jiang, Qingyun Li, Xue Yang,
 694 and Wayne Zhang. Geoground: A unified large vision-language model for remote sensing visual
 695 grounding. *arXiv preprint arXiv:2411.11904*, 2024b.

696

697 Qi Zhu, Jiangwei Lao, Deyi Ji, Junwei Luo, Kang Wu, Yingying Zhang, Lixiang Ru, Jian Wang,
 698 Jingdong Chen, Ming Yang, Dong Liu, and Feng Zhao. Skysense-o: Towards open-world re-
 699 mote sensing interpretation with vision-centric visual-language modeling. In *Proceedings of the*
 700 *Computer Vision and Pattern Recognition Conference (CVPR)*, pp. 14733–14744, June 2025.

701

702 **A THE USE OF LARGE LANGUAGE MODELS**
703704 The LLMs were used in three ways: (i) to edit and polish grammar and phrasing; (ii) using “Deep-
705 Research” to help retrieve and cluster related literature (with all citations verified by the authors).
706 We reviewed, verified, and take full responsibility for the contents.
707708 **B REPRODUCIBILITY STATEMENT**
709710 We are committed to ensuring the reproducibility of our research. When we trained the SFT model,
711 GRPO model and DAPO model, all the random seeds are fixed. Our implementation is built upon
712 VLM-R1 and Easy-R1 codebase. All datasets used in our experiments, such as VRSBench, NWPU,
713 EarthReason, RRSIS-D, and DIOR-RSVG, are publicly available. All models, training recipes will
714 be open-sourced in <http://geo-r1.github.io> to make sure the results presented in our main
715 paper are reproducible.
716717 **C PROMPT TEMPLATE**
718719 We largely follow the VLM-R1 prompt templates for REC, OVD, and extend the same interface to
720 the GRES setting. We append the thinking template at the end for all task prompts.
721722 **Prompt Template of REC**723 *Please provide the bounding box coordinates of the region this sentence describes: {query}.*
724725 **Prompt Template of OVD**726 *Please carefully check the image and detect the following objects: {target list}. Output
727 each detected target’s bbox coordinates in JSON format. The format of the bbox coordinates is:*728

```
729     ````json
730     [
731     {
732         "bbox_2d": [x1, y1, x2, y2],
733         "label": "category name"
734     },
735     {
736         "bbox_2d": [x1, y1, x2, y2],
737         "label": "category name"
738     }
739     ]
740     ````
```

741 *If there are no such targets in the image, simply respond with None.*
742743
744
745
746
747
748
749
750
751
752
753
754
755

756
757**Prompt Template of GRES**758
759
760

Please carefully check the image and answer: `{query}`. Based on your answer, detect all relevant objects in the image. Output each detected target's bbox coordinates in JSON format. The format of the bbox coordinates is:

761
762
763
764
765
766
767
768
769
770
771
772
773
774

```
```json
[
{
 "bbox_2d": [x1, y1, x2, y2],
 "keypoint1": [x3, y3],
 "keypoint2": [x4, y4]
},
{
 "bbox_2d": [x1, y1, x2, y2],
 "keypoint1": [x3, y3],
 "keypoint2": [x4, y4]
}
]
```

```

775

Thinking Template776
777
778
779

`{problem}` Output the thinking process in `<think>` `</think>` and final answer in `<answer>` `</answer>` tags.

780
781
782
783
784
785
786
787**D DEMO**

We visualize the model's reasoning process for demonstration. Figure 5 shows some successful case on GRES task, while Figure 6 illustrates examples on GREC tasks. In general, Geo-R1 is able to provide a reasonable thinking process that leads to the accurate answer.

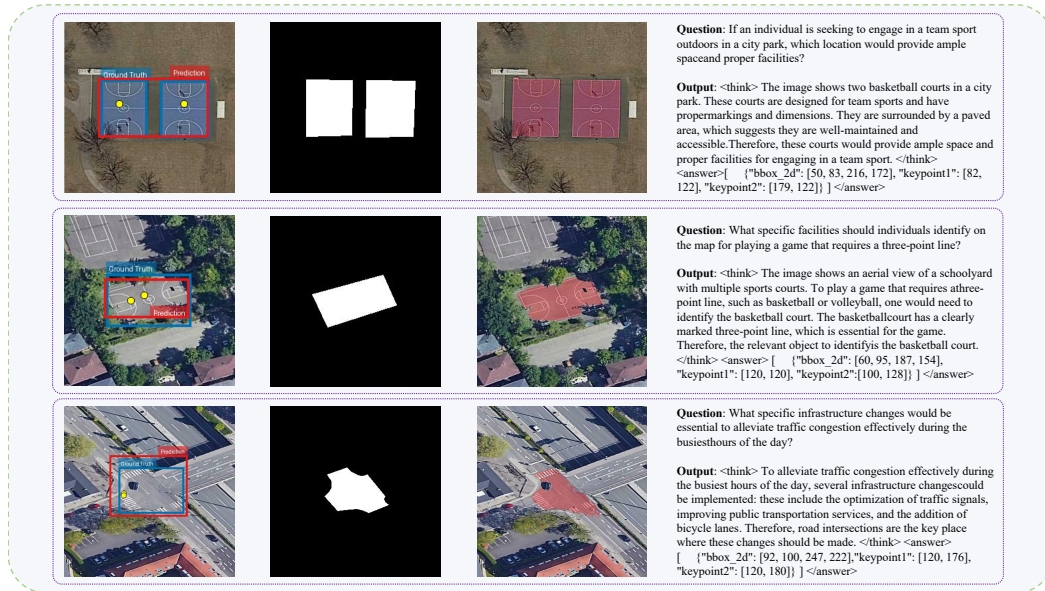
788
789
790
791
792
793
794
795
796
797
798
799
800
801
802
803
804
805
806
807
808
809

Figure 5: Geo-R1 inference samples (success case for GRES).

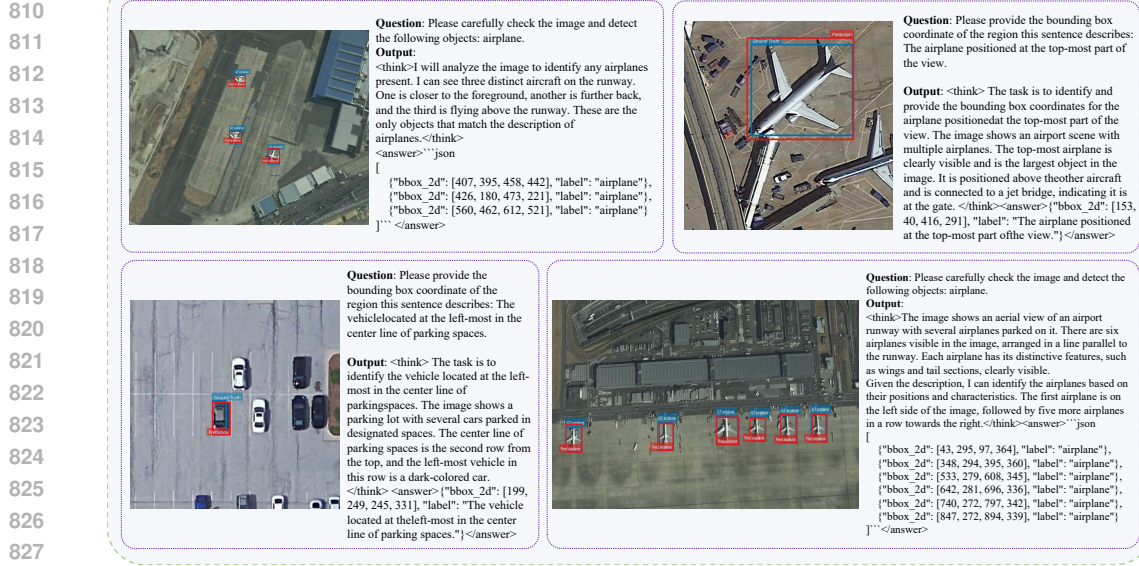


Figure 6: Geo-R1 inference samples (success case for GREC).

830
831
832
833
834
835
836
837
838
839
840
841
842
843

In general, Geo-R1 is able to provide a reasonable thinking process that leads to an accurate answer. However, we also identify key failure modes that highlight a disconnect between an often-plausible reasoning process and the final spatial output.

As shown in the top-left of Figure 7, the model can correctly reason in its reasoning process that the park area is the most suitable region for wildlife preservation, yet its final answer incorrectly grounds this concept to the nearby sports facility. In the bottom-right example, the model’s reasoning correctly identifies the presence of multiple ships, but the final answer detects only the cluster on the left while omitting the group on the right. Furthermore, we also observe failures in reasoning process, the bottom-left example shows a failure within the reasoning process itself. Although the model accurately understands the task in its reasoning block (to identify the ‘large vehicle’), it subsequently fails to apply this critical size attribute, incorrectly selecting a much smaller, adjacent vehicle for its final answer. These cases suggest that a key area for future improvement is strengthening the alignment between the model’s high-level semantic understanding and the generation of accurate, complete, and precise spatial coordinates.

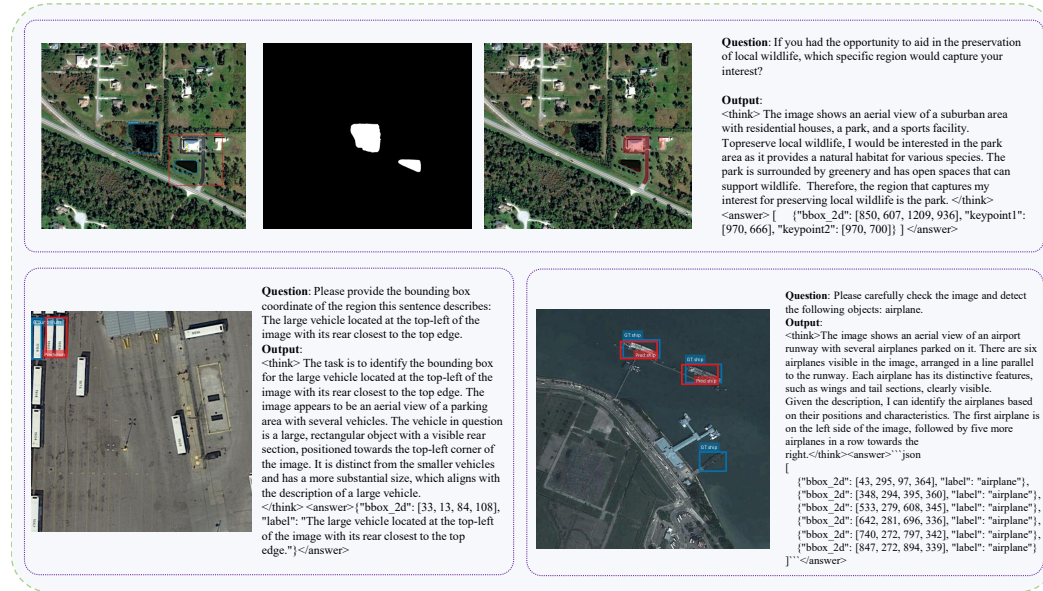


Figure 7: Geo-R1 inference samples (failure case).

864 **E ADDITIONAL EXPERIMENTS**
865866 **E.1 ABLATION STUDY ON FORMAT REWARD**
867868 Table 6 shows that without the format reward, Geo-R1 exhibits slightly degraded performance on
869 both REC and GRES tasks. Empirical results also show that Geo-R1 w/o format reward requires
870 much longer training time to converge (about 1.6x longer for REC, 1.7x longer for OVD and 1.3x
871 longer for GRES) compared to Geo-R1 w/ format reward.
872873 **Table 6: Ablation on Format Reward.**
874

| | REC (Acc@0.5) | GRES-val (gIoU) | GRES-test (gIoU) | OVD (mAP) |
|--------------------------|---------------|-----------------|------------------|-----------|
| Geo-R1 w/ format reward | 50.59 | 57.78 | 58.27 | 34.92 |
| Geo-R1 w/o format reward | 48.23 | 56.61 | 57.24 | 34.64 |

880 **E.2 ABLATION STUDY ON PENALTY OF OVERLONG OVD PREDICTION RESULT**
881882 Table 7 shows that without the length penalty reward, Geo-R1 exhibits significantly degraded per-
883 formance on the OVD task.
884885 **Table 7: Ablation on Length Penalty of OVD task.**
886

| | OVD (mAP) |
|---------------------------|-----------|
| Geo-R1 w/ length penalty | 34.92 |
| Geo-R1 w/o length penalty | 27.52 |

892 **E.3 VARIANCE AND ROBUSTNESS REPORT**
893894 The few-shot training samples were randomly selected. To further assess robustness with respect to
895 shot selection, we re-sampled the training data using different random seeds and re-ran the experi-
896 ments for the REC and GRES tasks. For OVD, we re-sampled with 3 different random seeds due
897 to time constraint and report 5-shot result (10-shot setting for OVD is hard to re-sample different
898 samples). As shown in the Table 8, our model exhibits stable performance across 10 different seeds,
899 with standard deviations below 1%.
900901 **Table 8: Robustness with Different Few-shot Samples.**
902

| Task | Metrics | Reported (Seed 42) | Average \pm std | Seed 43 | Seed 44 | Seed 45 | Seed 46 | Seed 47 | Seed 48 | Seed 49 | Seed 50 | Seed 51 | Seed 52 |
|-----------|---------|--------------------|-------------------|---------|---------|---------|---------|---------|---------|---------|---------|---------|---------|
| REC | Acc@0.5 | 50.59 | 49.46 \pm 0.95 | 49.90 | 49.76 | 50.34 | 49.77 | 50.28 | 47.43 | 49.20 | 49.61 | 50.33 | 47.99 |
| GRES-Val | gIoU | 57.78 | 59.19 \pm 0.31 | 59.08 | 58.78 | 59.41 | 59.58 | 59.57 | 58.80 | 59.33 | 59.52 | 58.89 | 58.94 |
| GRES-Test | gIoU | 58.27 | 58.05 \pm 0.63 | 59.00 | 58.20 | 58.18 | 57.27 | 58.41 | 57.10 | 58.47 | 58.59 | 58.17 | 57.11 |
| OVD | mAP | 33.20 | 34.29 \pm 0.45 | 34.36 | 33.71 | 34.79 | | | | | | | |

906 **E.4 ADDITIONAL RESULT FOR REC TASK (OPT-RSVG DATASET)**
907908 To validate the effectiveness of Geo-R1, we further test the Geo-R1 on OPT-RSVG (Li et al., 2024a)
909 dataset under a zero-shot setting. SFT baseline is compared, and we report the Acc@0.5. Result can
910 be seen in Table 9. From this Table, our Geo-R1 model shows significantly better performance than
911 the SFT counterpart.
912913
914
915
916
917

918
919
920
921
922
923
924
925
926

Table 9: REC Result on OPT-RSVG Dataset.

| | Val | Test |
|--------|-------|-------|
| SFT | 30.24 | 31.06 |
| Geo-R1 | 33.76 | 34.29 |

E.5 THINKING V.S. NOT THINKING

We provide RFT results with and without thinking in Table 10. Overall, RL training with thinking provides slightly better performance and much better interpretability. Moreover, RFT consistently outperforms SFT regardless of whether thinking is applied.

E.6 PARAMETER EFFICIENT FINETUNING FOR GEO-R1

we train our Geo-R1 model using LoRA (rank = 64, alpha = 128), and the results are shown in the Table 11 below. Results show that combining LoRA with Geo-R1 slightly hurts the performance and does not save much training time compared with full fine-tuning (9 hours vs. 10 hours). This is because the rollout operation dominates the GRPO training process, while updating the LLM accounts for only a small portion of the total time.

Table 11: Parameter Efficient Finetuning for Geo-R1.

| | REC (Acc@0.5) | GRES-val (gIoU) | GRES-test (gIoU) |
|----------------------|---------------|-----------------|------------------|
| Geo-R1 LoRA | 47.62 | 51.46 | 53.89 |
| Geo-R1 full-finetune | 50.59 | 57.78 | 58.27 |

E.7 COMPARISON WITH OTHER APPROACHES.

We add a comparison, Grounding-DINO (Liu et al., 2024c), for REC task. Specifically, the Grounding-Dino-T is fine-tuned with 10-shot and 5-shot REC data for 30 epoch, using Open-Grounding-Dino framework⁴. The result can be seen in Table 12.

Table 12: Comparison with Other Approaches.

| | 10-shot | 5-shot | 1-shot |
|----------------|---------|--------|--------|
| Grounding-DINO | 37.65 | 26.52 | 22.51 |
| Qwen2.5-VL-SFT | 38.29 | 35.21 | 32.75 |
| Geo-R1 | 50.59 | 47.62 | 45.78 |

⁴<https://github.com/longzw1997/Open-GroundingDino>

972

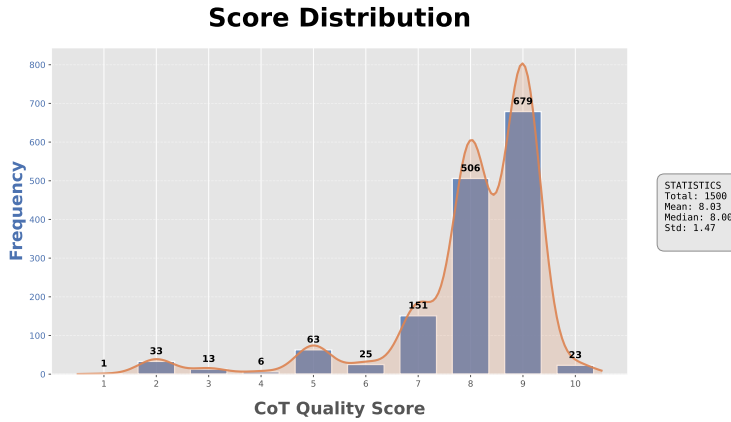
973

E.8 ASSESSMENT ON GENERATED REASONING CHAINS

974
975
976
977
978
979
980

To further validate reasoning quality, we conducted an additional analysis in which we prompted Qwen3-VL-235B-A22B-Thinking⁵ to automatically evaluate a randomly sampled subset of reasoning chains whose corresponding predictions have $\text{IoU} > 0.5$ on the VRSBench test set (1500 samples). We carefully designed prompts to assess both the correctness and usefulness of the reasoning toward the final prediction, assigning score on a 1–10 scale. As summarized in the Figure 8, the average reasoning quality score is 8.03 with std of 1.47, indicating that the majority of generated reasoning chains are reasonable, informative, and supportive of the final predictions.

981
982
983
984
985
986
987
988
989
990
991
992
993
994



995

996

Figure 8: Statistics of Quality Assessment on Generated Reasoning Chains.

998
000

CoT Quality Evaluation Prompt

1000
1001
1002

You are a strict evaluator for a vision–language model that performs **referring expression comprehension (visual grounding)** on remote sensing images.

1002

For each sample, you will be given:

1000
1001
1002
1003
1004
1005
1006
1007
1008
1009
1010
1011

- `image`: a remote sensing / aerial image.
- `question`: a natural-language referring expression describing a target region.
- `ground_truth`: the correct bounding box of the referred region: `[x_min, y_min, x_max, y_max]`.
- `model_output`: the model's full output, which contains:
 - a reasoning **Chain-of-Thought** between `<think> ... </think>`,
 - a final JSON-style prediction between `<answer> ... </answer>` with a predicted bbox `bbox_2d`.
- `extracted_answer`: the predicted bbox `[x_min, y_min, x_max, y_max]` parsed from the final answer.
- `correct`: whether the final prediction is counted as correct (1 or 0).

1016
1017
1018

Your job: **only evaluate the reasoning text inside <think> . . . </think> and output a single overall quality score from 1 to 10 (higher is better).**

You should internally consider two aspects:

1020

1. **Correctness** of the reasoning.
2. **Usefulness** of the reasoning.

1022

But your final output must be just **one combined score** that reflects both.

Do **not** change the model's prediction. Do **not** generate a new bounding box.

⁵<https://github.com/QwenLM/Qwen3-VL>

1026

1027

1028

1029

1030

1031

1032

1033

1034

1035

1036

1037

1038

1039

1040

1041

1042

1043

1044

1045

1046

1047

1048

1049

1050

1051

1052

1053

1054

1055

1056

1057

1058

1059

1060

1061

1062

1063

1064

1065

1066

1067

1068

1069

1070

1071

1072

1073

1074

1075

1076

1077

1078

1079

1. Criterion to Consider When Scoring

1.1. Correctness

Correctness measures how **factually accurate and logically sound** the reasoning is, relative to:

- the image content,
- the question / referring expression,
- the ground-truth bounding box and the predicted bounding box.

Key points:

1. Visual faithfulness

- The reasoning should accurately describe what is visible (object categories, spatial relations, comparative relations, etc.).
- Penalize:
 - referring to objects that do not exist in the image,
 - clearly wrong locations (e.g., calling a top-left object “bottom-right”),
 - confusing object types (e.g., calling a tennis court a baseball field).

2. Consistency with ground-truth and prediction

- Use `ground_truth` and `extracted_answer` to understand which region is correct and how close the prediction is.
- If the predicted bbox is near the ground truth and the reasoning clearly supports this localization, correctness should be **high**, as long as there are no serious hallucinations.
- If the predicted bbox is far from ground truth and the reasoning is based on the wrong object/region, correctness should be **low**, even if the text is fluent.

3. Logical consistency

- The reasoning should be internally coherent:
 - no self-contradiction (e.g., first says “top-left” then “bottom-right” for the same object),
 - no obvious contradiction with the predicted bbox (e.g., reasoning says the object is “top-left” but the predicted box is in bottom-right).

Rule: If correctness is extremely low (e.g., the reasoning clearly focuses on a completely wrong object or is mostly hallucinated), the final overall score must also be low (around 1–3), no matter how nicely written it is.

1.2. Usefulness

Usefulness measures how **helpful and informative** the reasoning is for explaining **why** the model chose the final bounding box.

Key points:

1. Task-specific grounding

- A useful CoT clearly connects the question to the image:
 - identifies candidate objects that match the category (ships, vehicles, fields, buildings, etc.),
 - compares positions (left-most, bottom-most, near center, near boundary, etc.),
 - uses context (e.g., “among the ships”, “in the bottom-left corner”, “between two runways”, “inside the stadium”, “on the water, not on land”).
- Penalize:
 - CoT that just paraphrases the question without adding visual evidence,
 - very generic lines (“I look at the image and find the object described”) with no actual reasoning.

2. Conciseness and relevance

- Prefer reasoning that is focused on the grounding task.

1080
1081
1082
1083
1084

- Penalize:
 - very long but repetitive reasoning that adds no extra information,
 - completely off-topic storytelling.

1085
1086
1087
1088

2. How to Combine into a Single Score (1–10)

You must convert your internal judgment about correctness and usefulness into a **single integer score from 1 to 10**.

1089
1090
1091
1092
1093
1094
1095
1096
1097
1098
1099
1100
1101
1102
1103
1104
1105
1106
1107
1108

Use the following guidelines:

- **9–10 (Excellent overall quality):** reasoning is highly correct (no major factual or spatial mistakes, no hallucinations, strongly aligned with the correct region) and highly useful (explicitly ties language to visual evidence, considers candidates, compares positions, and explains why the final region is chosen). This is the kind of CoT you would want as a **gold standard teaching signal**.
- **7–8 (Good overall quality):** reasoning is mostly correct, with at most minor inaccuracies or slight vagueness. It is useful but may miss some steps or be less detailed (e.g., fewer explicit candidate comparisons). Still clearly grounded and helpful.
- **4–6 (Mixed / moderate quality):** reasoning is partially correct (right general area or object type) but has notable gaps, imprecision, or some incorrect statements. Usefulness is limited: some connection between question and image exists, but the explanation is shallow, generic, or incomplete. This range also includes cases where the CoT is well structured but correctness is only moderate.
- **1–3 (Poor overall quality):** reasoning is mostly incorrect or hallucinated, focusing on the wrong object or contradicting obvious visual evidence, or is so vague/generic that it provides almost no real grounding. Even if the final predicted bbox happens to be correct, if the CoT is wrong or useless, the score must remain low.

3. Evaluation Procedure

For each sample:

1109
1110
1111
1112
1113
1114
1115
1116
1117
1118
1119
1120
1121
1122
1123
1124

1. **Understand the target:** read the question to understand what region is being referred to (e.g., “left-most ship”, “top-center soccer field”, “vehicle at bottom-right”, “bridge in the middle”).
2. **Inspect ground-truth and prediction:** use `ground_truth` and `extracted_answer` to understand which region is correct and which region was chosen by the model. This helps you judge if the reasoning aligns with the proper region.
3. **Read the CoT inside <think>...</think>:** ignore anything outside `<think>...</think>` for scoring. Evaluate how correct and how useful this reasoning is as described above.
4. **Assign a single overall score (1–10):** combine correctness and usefulness as described in Section 2. Also provide a brief explanation of why you chose this score.

4. Output Format

Return your evaluation as a **Python-style dictionary literal**, with no extra text:

1125
1126
1127
1128
1129
1130
1131
1132
1133

```
{
  "score": <integer 1-10>,
  "explanation": "<1-3 short sentences explaining your
  judgment of correctness and usefulness together>"
}
```